ELSEVIER

Journal of Nuclear Materials 306 (2002) 213–217

journal of nuclear materials

www.elsevier.com/locate/jnucmat

Experimental verification of the existence and structure of ζ Pu_6Fe in a Pu–Ga alloy

K.T. Moore, M.A. Wall, A.J. Schwartz *

Lawrence Livermore National Laboratory, Chemistry and Materials Science Directorate, L-355, Livermore, CA 94550, USA

Received 20 June 2002; accepted 30 September 2002

Abstract

A phase belonging to the space group *I*4/*mcm* was identified in a Pu–Ga alloy containing trace amounts of Fe and Ni using electron diffraction and energy-dispersive X-ray spectroscopy (EDXS) in a transmission electron microscope. The plane group symmetry of six experimental diffraction patterns showed that the structure of this phase was at least body-centered orthorhombic. Simulated diffraction patterns, generated from the body-centered tetragonal structure of ζ Pu_6Fe with the space group *I*4/*mcm*, match the experimental diffraction patterns closely. These results present the first crystallographic evidence for the existence of ζ Pu_6Fe in a dilute Pu–Ga alloy. The Pu/Fe ratio of the phase yielded by EDXS was 12.5 at.% and the Pu/(Fe + Ni) ratio was 15.9 at.%. These results suggest that Ni substitutes for Fe in the ζ, Pu_6Fe lattice.

1. Introduction

The interaction between Pu and Fe is of considerable importance for many technological applications. For example, reactions occur between metallic U–Pu–Zr fuel for fast reactors and the stainless steel cladding used to house the fuel [1,2]. The importance of understanding the reactions between Pu with Fe in particular is exacerbated due to the existence of a low-melting-point eutectic in the Pu-rich side of the phase diagram (see Fig. 1 [3]), which creates potential safety hazards. The eutectic occurs because of a low-melting-temperature intermetallic phase, ζ Pu_6Fe.

ζ Pu_6Fe was first discovered in Konobeevsky by 1955 [4]. Using X-ray diffraction (XRD), ζ Pu_6Fe was determined to be body-centered tetragonal (space group *I*4/*mcm*), where $a = b = 1.0405$ nm and $c = 0.5349$ nm. This structure was later confirmed by Coffinberry and Ellinger [5] and Mardon et al. [6] with XRD during attempts to determine the entire Pu–Fe phase diagram. In the above experiments ζ Pu_6Fe was formed by melting specific ratios of Pu and Fe for the purpose of delineating the Pu–Fe phase diagram. In the present research ζ Pu_6Fe was identified in a Pu–Ga alloy, which contained trace amounts of Fe and Ni.

Two precipitates approximately 2–3 μm in size were examined in an fcc δ phase Pu–Ga alloy using electron diffraction and energy-dispersive X-ray spectroscopy (EDXS) in a transmission electron microscope (TEM). The precipitates were determined to be body-centered tetragonal with the space group *I*4/*mcm* by employing simulated and experimental electron diffraction. Additionally, EDXS revealed that the Pu/Fe ratio was 12.5% and the Pu/(Fe + Ni) ratio was 15.9%, both very close to the 14.3% expected due to stoichiometry. The presence of a ζ Pu_6Fe phase in Fe-containing Pu–Ga alloys has been suggested on the basis of electron microprobe and optical microscopy investigations. However, there has never been any crystallographic evidence for the existence of this phase in Pu–Ga alloys. The present results

* Corresponding author. Tel.: +1-925 423 3454; fax: +1-925 424 4737.

E-mail address: schwartz6@llnl.gov (A.J. Schwartz).

0022-3115/02/$ - see front matter © 2002 Published by Elsevier Science B.V.
PII: S0022-3115(02)01319-3

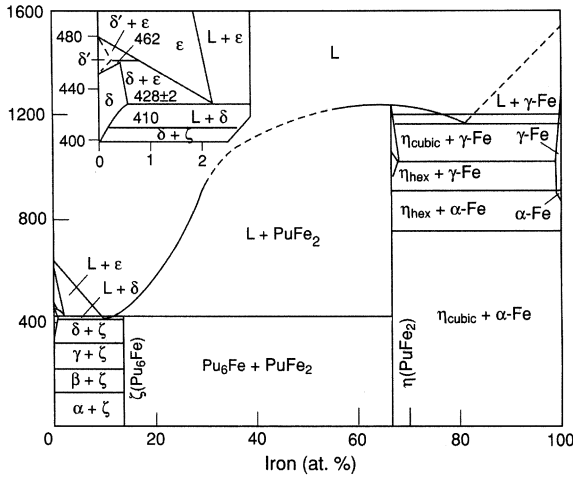

Fig. 1. The Pu–Fe binary phase diagram [3]. The line compound examined in the present paper, ζ Pu_6Fe, can be seen near 14 at.% Fe. Notice the extremely small or non-existent solubility of Fe in solid Pu.

add to ongoing research of Pu alloys [7], and represent the first observed occurrence of ζ Pu_6Fe in a Pu–Ga alloy that contains trace amounts of Fe and Ni.

2. Experimental procedures

TEM samples were prepared from bulk Pu–Ga material following the procedure described by Wall et al. [8]. Special care was taken throughout the process to prevent any significant temperature rise or stress in the material and in the specimens extracted from it. Samples 31.75-mm in diameter were obtained by single point milling with trichloroethylene (TCE) steady drip lubricant. The disk was sectioned in thirds using a low speed diamond saw flooded with Dow Corning 200 cutting fluid. To insure minimal heating, the low speed diamond saw was again used to cut 6.5-mm squares from nearest the center of the original disk. These squares were mounted on a 6.5-mm diameter aluminum rod, secured in the lathe, and turned to 2.8-mm diameter with 0.05-mm reductions per pass and TCE coolant. For final specimen preparation, the samples were moved to a dry train recirculating glove box with a base line environment of ≈1 ppm for O_2 and ≈1 ppm for H_2O with an inert atmosphere of nitrogen. The cylindrical specimen was sliced to 1.0-mm thickness before lapping on 30-μm, 12-μm, then 3-μm aluminum oxide paper. Thin foils for TEM observation were made by electropolishing in a solution of 10% nitric acid (70% concentration), 45% methanol and 45% butoxyethanol (butylcellusove) by volume. The parameters for electropolishing were as follows: −20 °C, 35 V and ≈40 mA. The specimen was thinned continuously to perforation. After perforation, the sample is immediately re-polished at a higher voltage (50 V) for 2–3 s to remove a thin anodic film that develops during the continuous polishing at lower voltages. The sample was then rinsed in the holder with methanol (anhydrous), followed by removal of the specimen from the holder placing the specimen in methanol. The sample was rinsed in several baths of methanol for approximately 1 min each then rinsed and stored in 200 proof ethanol until ready to transfer to the TEM. A vacuum transfer specimen holder was used for containing the specimen and maintaining the Ar environment.

Imaging and diffraction experiments were performed using a Philips CM300 FEG TEM operating at 297 kV. Zero-loss filtered images and diffraction patterns were digitally acquired using a Gatan imaging filter with a charge-coupled-device camera with a 2048 pixels × 2048 pixels array. Zero-loss filtering removes inelastic electron scatter, leaving intensity due only to elastic scatter. This yields images and diffraction patterns that are sharper and reveal more information.

Simulated diffraction patterns were produced using both EMS online (http://cimesg1.epfl.ch/CIOLS/crystal1.pl) and the tandem package of CrystalKit and MacTempas. Sample thickness was determined using the electron energy-loss spectroscopy log-ratio technique [9]. Using this technique, the sample thickness in the region examined was determined to be 50 ± 5 nm. Simulations were performed under dynamical conditions for a sample thickness of 50 nm. The unit cell used for diffraction pattern simulations was space group 140 with $a = b = 1.041$ nm and $c = 0.535$ nm and the basis, Pu: 0.4068, 0.9068, 0 and 0.2141, 0.121, 0 and Fe: 0, 0, 0.25 [4].

EDXS spectra were acquired using the CM300 with an Oxford ultra-thin window detector and an XP3 pulse processor. Spectra were acquired with the sample tilted approximately 20° toward the detector to ensure optimum counting statistics. Additional collection parameters are: take-off angle ≈ 35°, 1.0 nm beam diameter, count rate ≈ 2000 cts/s, acquisition time ≈ 100 s/point with four points total. After the spectra were acquired an in-hole count under the same conditions was acquired to record the self-emission of radiation from the sample. This in-hole spectra was subtracted from the specimen spectra prior to spectra processing. Quantification was performed using the K-ratio method of Cliff and Lorimer [10]. A K-ratio for the Pu $L_{\alpha 1}$ to Fe $K_{\alpha 1}$ of 0.323 was used. The K-ratio was partially determined experimentally from a Pu–Ga alloy and a calculated K-ratio of Ga $K_{\alpha 1}$ to Fe $K_{\alpha 1}$ using Thin-Film Analysis (v. 1.3). The experimental determination of the Fe/Ni to Pu concentration is limited to ≈10% error because of the uncertainty of knowing the Pu–Ga alloy concentration.

3. Results

Two lens shaped precipitates approximately 2–3 μm in length were observed in the fcc δ Pu matrix. One of these lenses is shown in the bright-field TEM image in Fig. 2. The edge of the precipitate, which is arrowed in Fig. 2, can be discerned by the termination of bend contours at the precipitate–matrix interface and by slight differences in overall diffraction intensity between the precipitate and matrix. Foil bending in the vicinity of the edge is readily observed by the nature of the bend contours.

EDXS spectra taken from the matrix and precipitate are shown in Fig. 3(a) and (b), respectively. The spectrum from the Pu matrix (b) displays both a Pu and a Ga peak in EDXS spectra, as expected. Additionally, there are Np and U peaks due to decay of the Pu and a Cu peak due to the Cu sample cup. The spectrum from the precipitate contains a considerable Fe peak and a smaller Ni peak, but no Ga. Quantification of EDXS spectra revealed that the Pu/Fe ratio was 12.5 at.% and the Pu/(Fe + Ni) ratio was 15.9 at.%. These are both very close to the 14.3 at.% expected for Pu_6Fe due to stoichiometry, and suggest that Ni is substituting for Fe in the lattice. Notice that no Fe is detected in the matrix, which is reasonable since Fe has very little solubility in α, β, and γ Pu and moderate solubility in δ and ε Pu (see Fig. 1) [3,6]. Because the precipitate was obviously not δ Pu on the grounds of composition, a number of diffraction patterns were acquired from the precipitate to discern the crystal structure.

A set of experimental diffraction patterns acquired from one of the precipitates is shown in Fig. 4 accompanied by a [1 $\bar{1}$ 0] stereographic projection revealing the spatial relationship of the poles. [1] Six experimental diffraction patterns taken from the precipitate appear along the left and top side of Fig. 4. The orientations are [2 $\bar{3}$ 0], [1 $\bar{1}$ 0], [3 $\bar{2}$ 0], [1 0 0], [2 0 $\bar{1}$], [1 0 $\bar{1}$], and some of the first and second-order reflections are indexed. Due to the plane group symmetry of the six patterns, which are c2mm, p2mm, c2mm, c2mm, c2mm, and p2mm, respectively, the unit cell is at least body-centered orthorhombic. Therefore, the diffraction patterns alone cannot prove the structure is tetragonal because the axis of fourfold symmetry was beyond the tilt of the microscope for both precipitates. However, by matching the six experimental diffraction patterns with simulated patterns generated from a unit cell of *I*4/*mcm* Pu_6Fe, the

[1] The α and β tilt of the sample in the microscope was recorded at each zone axis, plotted on a Wulff net, and compared to the calculated stereographic projection. The experimentally recorded angles between poles matched the simulated angles to within 3°. This slight discrepancy is explained by foil bending under the electron beam, which is evidenced in Fig. 2 by bend contours.

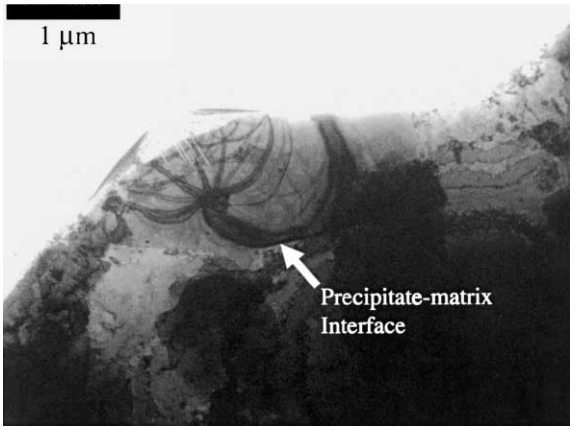

Fig. 2. A bright-field TEM image of one of the ζ Pu_6Fe precipitates contained in a fcc Pu matrix. The precipitate–matrix interface is marked with an arrow.

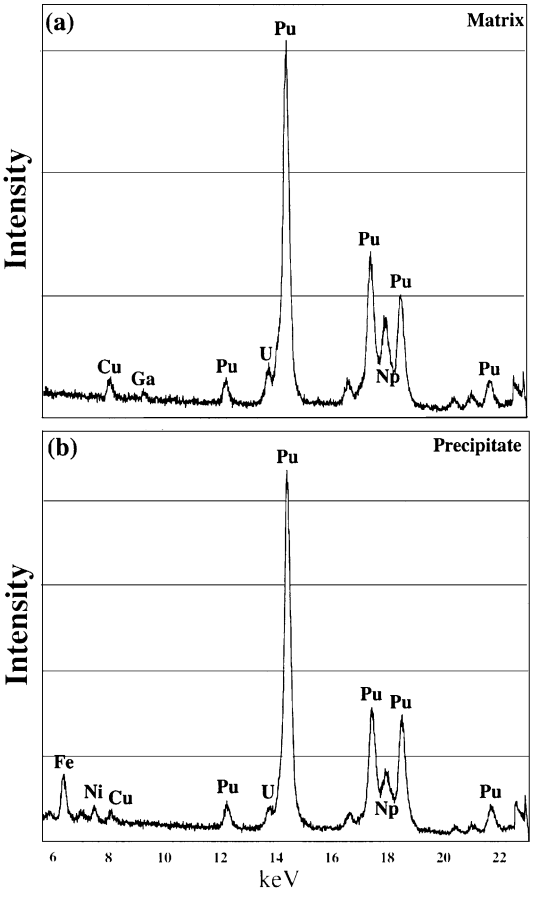

Fig. 3. Two EDXS spectra taken from; (a) the fcc Pu matrix and (b) one of the ζ Pu_6Fe precipitates. Notice that an Fe peak is found in the spectrum for ζ Pu_6Fe, but is absent in the spectrum for the Pu matrix.

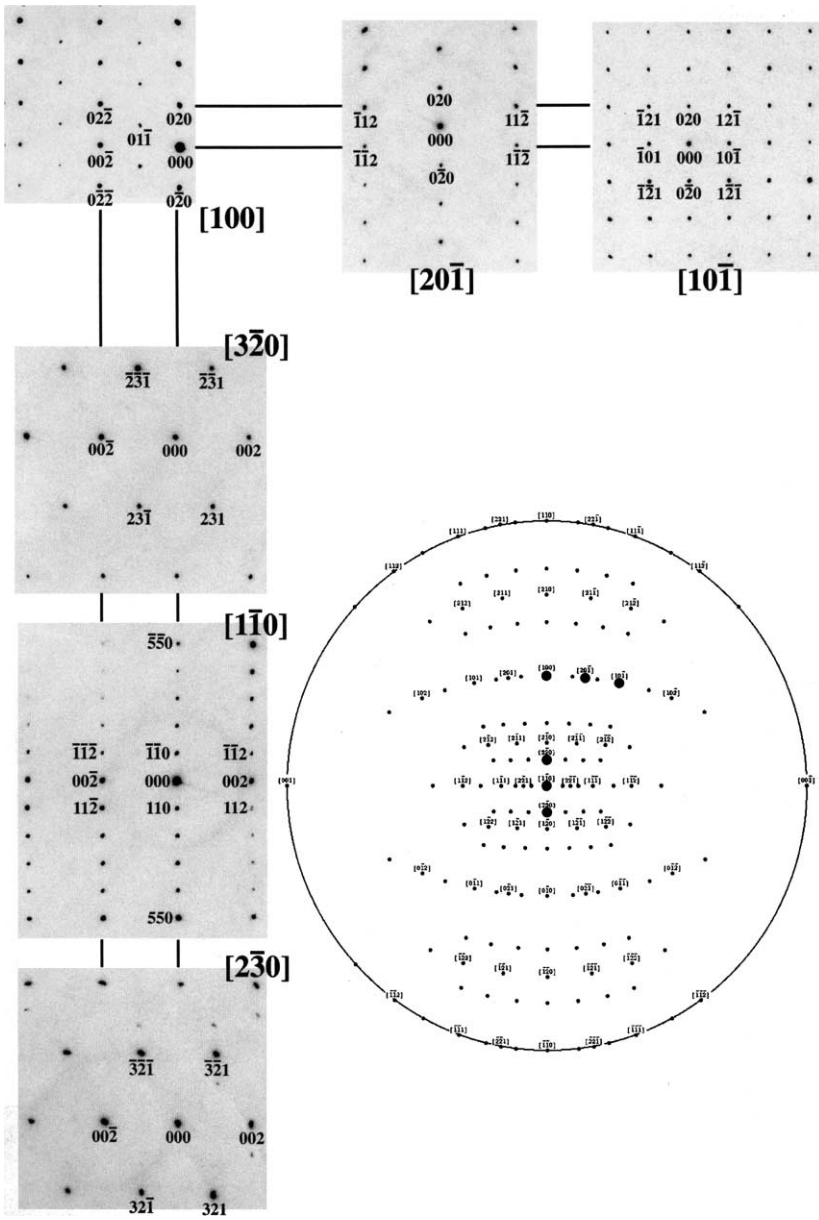

Fig. 4. A set of six experimental electron diffraction patterns taken from one of the ζ Pu_6Fe precipitates. A [1 $\bar{1}$ 0] stereographic projection is shown in the figure to demonstrate the spatial relationship of the poles to one another.

precipitate structure could be shown to be consistent with tetragonal Pu_6Fe.

Seven simulated diffraction patterns are shown in Fig. 5, which were generated using the body-centered tetragonal structure of Pu_6Fe with the space group $I4/mcm$. The patterns along the left and top side of Fig. 5 were simulated for a 50 nm thick sample under dynamical conditions, and are the same orientations as the experimental patterns in Fig. 4. The ratio of distance between reflections (relative) for each of the experimental patterns were compared to the simulated patterns and were within 1% error. The d-spacings (absolute) were within 2–3% error. By visual comparison it can be seen that the simulated patterns match the experimental patterns well. There are, however, a few exceptions. First, the experimental [1 $\bar{1}$ 0] pattern shows that the 55ℓ-type reflections are slightly more intense than other reflections. This was not observed in the simulated [1 $\bar{1}$ 0] pattern in Fig. 5. When simulations were performed using either a thinner sample (<5 nm)

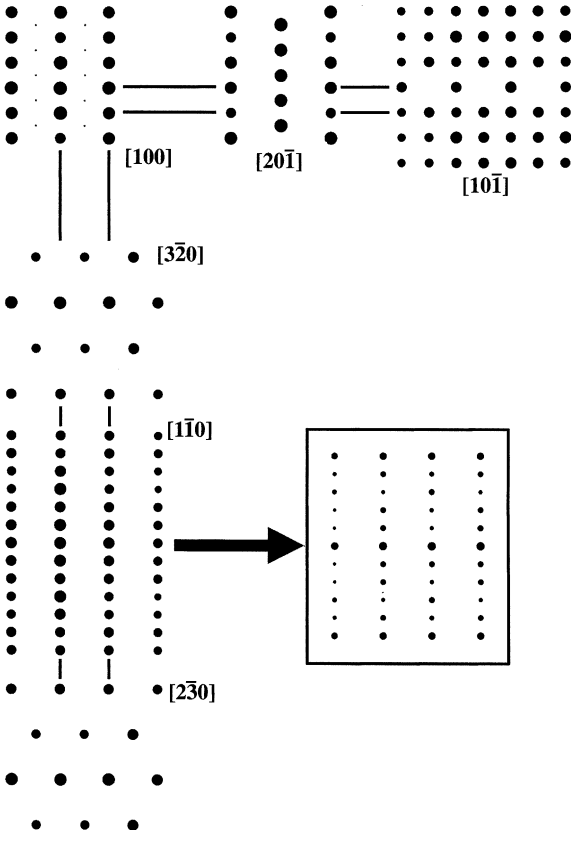

Fig. 5. A set of seven simulated electron diffraction patterns generated using a unit cell of ζ Pu_6Fe with space group $I4/mcm$. The six patterns along the left and top side of the figure are in the same orientation as the six experimental patterns in Fig. 4.

or kinematical conditions, the 55ℓ-type reflections became more intense, matching the experimental results. Second, the simulated [1 0 $\bar{1}$] diffraction pattern displayed a systematic absence of the $h0\ell$ reflections when $h =$ odd, due to the c glide plane. This systematic absence of reflections was not observed in the experimental diffraction pattern, but can be explained by double diffraction.

Convergent beam electron diffraction (CBED) was performed in a [1 $\bar{1}$ 0] zone axis orientation in an attempt to verify the axis of fourfold symmetry parallel to [0 0 1]. Assuming there is an axis of fourfold symmetry in the plane of the diffraction pattern and parallel to [0 0 1], then the 1 1 0 d-spacing should be equal both in the plane of the paper and in the direction of the electron beam. However, since Pu produces a large amount of thermal diffuse scattering, and we do not have the ability to cool the sample to LN_2 temperatures, quality CBED patterns could not be recorded.

4. Conclusions

Simulated and experimental electron diffraction patterns are consistent with the body-centered tetragonal Pu_6Fe phase. Additionally, EDXS spectra yield a Pu/Fe ratio of 12.5 at.% and the Pu/(Fe+Ni) ratio of 15.9 at.%, which suggest that Ni substitutes for Fe in the Pu_6Fe lattice. These results provide the first proof of the existence of ζ Pu_6Fe in Pu–Ga alloys that contain trace amounts of Fe and Ni.

Acknowledgements

Work performed under the auspices of the US Department of Energy by the University of California Lawrence Livermore National Laboratory under Contract W-7405-Eng-48.

References

[1] T. Ogata, K. Nakamura, M. Kurata, T. Yokoo, M.A. Mignanelli, J. Nucl. Sci. Tech. 37 (2000) 244.
[2] K. Nakamura, T. Ogata, M. Kurata, T. Yokoo, M.A. Mignanelli, J. Nucl. Sci. Tech. 38 (2001) 112.
[3] S.S. Hecker, Plutonium and its alloys – from atoms to microstructure, in: N.G. Cooper (Ed.), Challenges in Plutonium Science, Los Alamos Science, vol. II, Number 26, p. 317.
[4] S.T. Konobeevsky, in: Proceedings of a Conference on Peaceful Uses of Atomic Energy, Academy of Sciences USSR, Chemical Science Volume (English language edition), Consultants Bureau Inc., New York, 1955, p. 211.
[5] A.S. Coffinberry, F.H. Ellinger, in: Proceedings of the International Conference on Peaceful Uses of Atomic Energy, H.M. Stationary Office, New York, 1956, p. 138.
[6] P.G. Mardon, H.R. Haines, J.H. Pierce, M.B. Waldron, The Pu–Fe system, J. Inst. Met. Lond. 86 (1958) 166.
[7] B.D. Wirth, A.J. Schwartz, M.J. Fluss, M.J. Caturla, M.A. Wall, W.G. Wolfer, MRS Bull. 26 (9) (2001) 679.
[8] M.A. Wall, A.J. Schwartz, M.J. Fluss, Sample Preparation for Transmission Electron Microscopy Characterization of Pu Alloys, UCRL-ID-141746.
[9] T. Malis, S. Cheng, R.F. Egerton, J. Electron Microsc. 8 (1988) 193.
[10] G. Cliff, G.W. Lorimer, J. Microsc. 103 (1975) 203.